Journal of the Optical Society of America B
OPTICAL PHYSICS

# Mid-infrared emission in $Tb^{3+}$-doped selenide glass fiber

L. Sojka,[1,2] Z. Tang,[1] D. Furniss,[1] H. Sakr,[1] Y. Fang,[1] E. Beres-Pawlik,[2] T. M. Benson,[1] A. B. Seddon,[1] and S. Sujecki[1,2,*]

[1]Mid-Infrared Photonics Group, George Green Institute for Electromagnetics Research, Faculty of Engineering, University of Nottingham, University Park, Nottingham NG7 2RD, UK
[2]Telecommunications and Teleinformatics Department, Wroclaw University of Technology, Wybrzeze Wyspianskiego 27, 50-370 Wroclaw, Poland
*Corresponding author: slawomir.sujecki@nottingham.ac.uk

Received 3 October 2016; revised 8 February 2017; accepted 8 February 2017; posted 13 February 2017 (Doc. ID 276257); published 1 March 2017

**The mid-infrared (MIR) emission behavior of $Tb^{3+}$-doped Ge–As–Ga–Se bulk glasses (500, 1000, and 1500 ppmw $Tb^{3+}$) and unstructured fiber (500 ppmw $Tb^{3+}$) is investigated when pumping at 2.013 μm. A broad emission band is observed at 4.3–6.0 μm corresponding to $^7F_5 \rightarrow {}^7F_6$, with an observed emission lifetime of 12.9 ms at 4.7 μm. The $^7F_4$ level is depopulated nonradiatively and so it is proposed that $Tb^{3+}$-doped Ge–As–Ga–Se fiber may operate as a quasi-three-level MIR fiber laser. Underlying glass-impurity vibrational absorption bands are numerically removed to give the true $Tb^{3+}$ absorption cross section, as required for Judd–Ofelt (J–O) analysis. Radiative transition rates calculated from J–O theory are compared with measured lifetimes. A numerical model of the three-level $Tb^{3+}$-doped fiber laser is developed for $Tb^{3+}$ doping of $8.25 \times 10^{24}$ ions $m^{-3}$ (i.e., 500 ppmw) and dependence of laser performance on fiber length, output coupler reflectivity, pump wavelength, signal wavelength, and fiber background loss is calculated. Results indicate the feasibility of an efficient three-level MIR fiber laser operating within 4.5–5.3 μm, pumped at either 2.013 or 2.95 μm.**

Published by The Optical Society under the terms of the Creative Commons Attribution 4.0 License. Further distribution of this work must maintain attribution to the author(s) and the published article's title, journal citation, and DOI.

*OCIS codes:* (140.0140) Lasers and laser optics; (040.3060) Infrared; (060.2300) Fiber measurements; (060.2310) Fiber optics; (060.2390) Fiber optics, infrared; (140.3510) Lasers, fiber.
https://doi.org/10.1364/JOSAB.34.000A70

## 1. INTRODUCTION

Selenide-chalcogenide glasses have a phonon energy of ~300 $cm^{-1}$, a theoretical low optical-loss window of ~100 $dBkm^{-1}$ across ~3–10 μm in the mid-infrared (MIR) spectral region, and large refractive indices (~2.5–2.8). Hence, rare earth (RE) ions doped in a selenide glass host exhibit long radiative lifetimes and large absorption and emission cross sections [1]. Recently, we demonstrated small-core $Pr^{3+}$ -doped, selenide glass, step-index fibers (SIFs) in which the $Pr^{3+}$ lifetime remained the same (i.e., 7.8 ms at 4.7 μm, when pumped at 1.55 μm) as in the parent $Pr^{3+}$ -doped bulk glass, demonstrating a resistance to both RE-clustering and glass devitrification during the heat-treatment processing to make SIF [2]. Moreover, an exhaustive high-resolution transmission electron microscopy study found no glass devitrification in the fiber core and core/cladding interface. However optical loss, due to extrinsic scattering and absorption, must still be reduced. MIR fiber lasing has not yet been demonstrated beyond 3.9 μm [3]. One problem is the long lifetimes of adjacent RE electronic levels, in a selenide glass host, which tend to self-terminate, precluding lasing [4]. We have identified $Tb^{3+}$ as potentially not suffering from this problem. We show that in $Tb^{3+}$-doped Ge–As–Ga–Se glasses, when pumping into the $^7F_4$ level, the emission transitions from $^7F_4$, $^7F_3$, $^7F_2$, $^7F_1$, or $^7F_0$ levels are expected to be quenched and quickly relax to the long-lived $^7F_5$ manifold; quasi-MIR three-level laser action is then possible for the $^7F_5 \rightarrow {}^7F_6$ transition, i.e., from the first excited state to the ground state.

$Tb^{3+}$-doped chalcogenide-glass emission was first reported in 2001 [5]. Judd–Ofelt (J–O) modeling was applied in [6,7], assuming that the excited state $^7F_4$ was radiatively depopulated. However, experimental observation of strong emission has not been reported, to the best of our knowledge. Here, we have fabricated and measured absorption and emission of $Tb^{3+}$-doped Ge–As–Ga–Se bulk-glass samples (500, 1000, and 1500 ppmw $Tb^{3+}$) and fibers (500 ppmw $Tb^{3+}$) when pumping at 2.013 μm. In the transparent window of selenide glasses, near-infrared (NIR) and MIR fundamental vibrational absorption due to glass impurities tends to underlie, and be obscured by, the RE electronic absorption. The effect is

compounded because the extinction coefficients of fundamental vibrational absorption bands are some $10^5\times$ higher than for NIR overtone and combination vibrational absorption. Here, the true $Tb^{3+}$ absorption cross section was deconvoluted and used in (J–O) modeling [8]. Radiative transition rates and lifetimes, calculated from J–O theory, were compared with the experimentally observed lifetimes. Numerical modeling of the quasi-three-level $Tb^{3+}$-doped Ge–As–Ga–Se fiber laser was carried out to find the performance dependence on fiber length, output coupler reflectivity, pump wavelength, emission wavelength, and fiber baseline loss. Results indicated the feasibility of efficient three-level MIR fiber lasing within 4.5–5.3 μm, pumping at either 2.013 or 2.95 μm in $Tb^{3+}$-doped Ge–As–Ga–Se.

## 2. EXPERIMENTAL PROCEDURE

### A. Glass Melting

A 500 ppmw $Tb^{3+}$-doped Ge–As–Ga–Se glass rod was prepared and drawn directly to unstructured fiber of around 300–400 μm OD (outside diameter). Ge (5N purity, Materion), As (7N5, Furakawa Denshi, prior heat treated at $10^{-3}$ Pa), and Se (5N Materion, prior heat treated at $10^{-3}$ Pa) were batched inside a glovebox (MBraun: <0.1 ppm $H_2O$ and <0.1 ppm $O_2$) and melted at 850°C/12 h in a silica glass ampoule (prior air-baked and then vacuum-baked, each at 1000°C/6 h) before being quenched. Then gallium (Ga) (5N, Testbourne Ltd.) and terbium foil (3N, Alfa Aesar) were added and the glass remelted at 850°C/2 h in a silica glass ampoule (prior air-baked then vacuum-baked, each at 1000°C/6 h) before being quenched and annealed. The 1500 ppmw $Tb^{3+}$-doped bulk glass was prepared similarly, but the 1000 ppmw $Tb^{3+}$-doped bulk glass was prepared by one melting of all batched elements at 850°C/12 h. Actual parts per million by weight (ppmw) were within ±20 ppmw of the stated value.

### B. Linear Optical Properties

Absorption spectra across 0.6–10 μm of $Tb^{3+}$-doped Ge–As–Ga–Se bulk samples of a few millimeter optical path length, with input and exit faces ground parallel and polished to a 1 μm finish, were collected in a Bruker IFS 66/S Fourier Transform MIR Spectrometer, which had been purged to remove $CO_2$ and $H_2O$.

An improved Swanepoel method was used to measure the refractive index of thin films (30 μm thick) of the 500 ppmw $Tb^{3+}$-doped Ge–As–Ga–Se glass [9,10]. The thin film was prepared by hot pressing under vacuum ($10^{-5}$ Pa) of the 500 ppmw $Tb^{3+}$-doped Ge–As–Ga–Se glass fiber, annealing, and cooling. Therefore, the thin film was of the same glass composition as the bulk glass and the drawn fiber. However, the quenching rate affects glass density and hence refractive index. Therefore, we have calibrated our refractive index measurements; we have found agreement to within 0.65% for the same selenide glass composition, but in different forms, of a hot-pressed film (measured by the improved Swanepoel method) when compared to the minimum-deviation method using a polished prism of bulk glass at 12 wavelengths within the 1454–1574 μm band, at 10 nm intervals (Agilent fiber-coupled diode), and at 3.109 μm [interband cascade laser (ICL), NRL, USA].

### C. Emission Properties

Emission spectra were recorded at 300 K over 3–6.5 μm of $Tb^{3+}$-doped Ge–As–Ga–Se bulk glass and fiber, pumped at 2.013 μm, with a Tm:silica fiber laser (capable of 10 W output, LISA Laser) or at 1.940 μm, with a 500 mW multimode laser diode (BA-1940-E0500-MMF200 M2K). The fluorescence signal was modulated with a chopper (Scitec Instruments). The collected luminescence was focused onto the slit of a motorized Spex MiniMate monochromator with a diffraction grating blazed at 6 μm (51034 Jobian Yvon). Detection of the signal was achieved with a lock-in amplifier (EG&G Brookdeal 9503-SC), a room temperature MCT detector (Vigo System PVI-6), a preamplifier for the detector (Judson PA-6), a data acquisition card (NI USB-6008 National Instruments), and a computer. Emission was collected from bulk glasses across a polished sharp glass corner orthogonal to the pump and <1 mm from the incident pump beam, and to minimize photon trapping, using a distorted emission cross section and false elongation of emission-decay lifetimes [11]. The emission-decay lifetime at 4.7 μm in the $Tb^{3+}$-doped Ge–As–Ga–Se bulk glasses was collected with direct modulation of the 2.013 μm wavelength pump laser. Time evolution of the emission was monitored with a digital oscilloscope. The simplest single exponential fit was applied; we expect lifetime errors of <10%.

## 3. EXPERIMENTAL RESULTS

### A. Refractive Index Dispersion for $Tb^{3+}$-Doped Ge–As–Ga–Se Glass

Figure 1 shows the refractive index dispersion of 500 ppmw $Tb^{3+}$-doped Ge–As–Ga–Se thin film fitted to the Sellmeier formula:

$$n^2 = 1.485 + \frac{4.942\lambda^2}{\lambda^2 - 0.2923^2} + \frac{1.124\lambda^2}{\lambda^2 - 39.23^2}, \quad (1)$$

where $n$ is the refractive index and $\lambda$ is the wavelength. The sum of the standard error of the Sellmeier fit was $9.7445\times10^{-5}$ and $r^2 = 0.9991$.

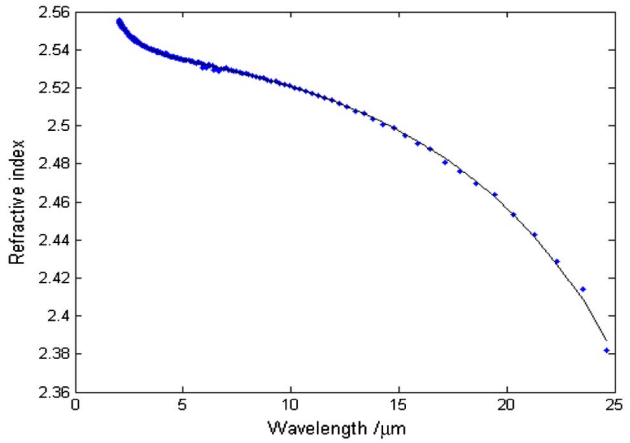


**Fig. 1.** Refractive index dispersion of 500 ppmw $Tb^{3+}$-doped Ge–As–Ga–Se (blue points are data points from the improved Swanepoel method, and the black curve is the Sellmeier fit to the data points).

### B. True Absorption Cross Section of $Tb^{3+}$

Figure 2(b) shows the electronic energy levels of $Tb^{3+}$-doped into the Ge–As–Ga–Se host based on the observed MIR absorption spectrum shown in Fig. 2(a) of the 500 ppmw $Tb^{3+}$-doped Ge–As–Ga–Se bulk glass, comprising six electronic absorption bands, centered at 1.5, 1.8, 2.0, 2.3, 2.95, and 4.65 μm, respectively, each originating from ground state, $^7F_6$, absorption of the $Tb^{3+}$ ions, to upper manifolds: $^7F_0$, $^7F_1$, $^7F_2$, $^7F_3$, $^7F_4$, and $^7F_5$, respectively. The $Tb^{3+}$ $^7F_6 \rightarrow {}^7F_0$ and $^7F_6 \rightarrow {}^7F_1$ absorption bands overlapped and were separated using Gaussian fitting [5].

The observed MIR absorption spectra of 500, 1000, and 1500 ppmw $Tb^{3+}$-doped Ge–As–Ga–Se bulk glasses (Fig. 3) belie the fact that hidden beneath the RE absorption bands is intrinsic and extrinsic absorption and scattering optical loss due to the host glass matrix and impurities. Sanghera *et al.* [12] have modeled intrinsic loss mechanisms of chalcogenide glasses and extrinsic loss mechanisms have been studied by the group of Churbanov (e.g., [13]). Underlying the $Tb^{3+}$ ground-state absorption, $^7F_6 \rightarrow {}^7F_4$, assumed centered at 2.95 μm, was found to be vibrational extrinsic absorption due to hydroxyl, i.e., -[O–H] contamination at ~2.7–2.9 μm. This hydroxyl tends to be bonded into the glass matrix in two ways, absorbing at two slightly different wavelengths (i) as hydroxide, e.g., [≡Ge–O–H], and (ii) as -[O–H] of molecular water, [H–O–H]. Underlying the $Tb^{3+}$ ground state absorption, $^7F_6 \rightarrow {}^7F_5$, assumed centered at 4.65 μm, was found to be vibrational extrinsic absorption due to [H–Se]- known to be centered at 4.6 μm [1].

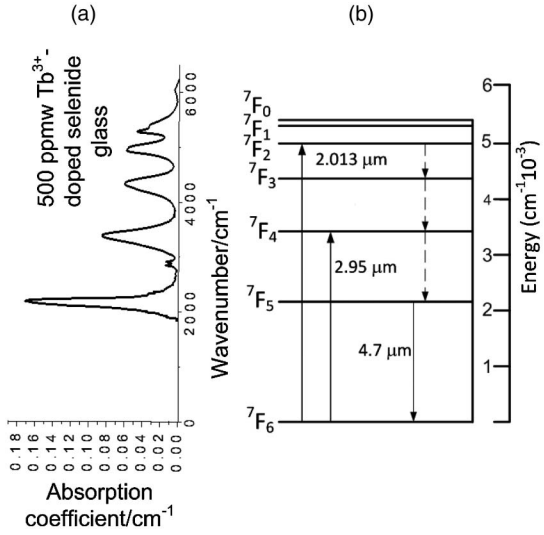


**Fig. 2.** (b) Simplified energy-level diagram for $Tb^{3+}$-doped chalcogenide glass proposed here according to (a) the absorption bands observed for $Tb^{3+}$ bulk samples using FTIR.

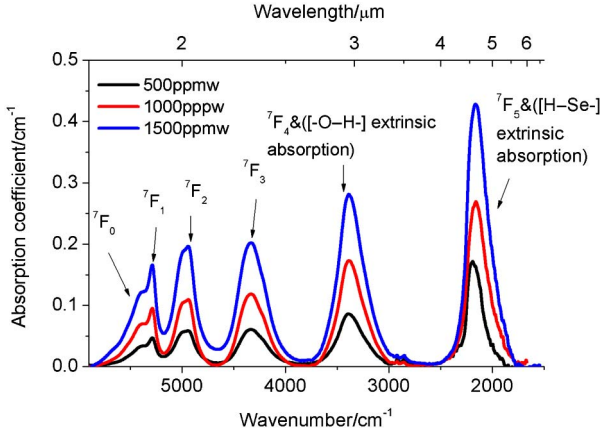


**Fig. 3.** Experimentally measured absorption spectra of 500, 1000, and 1500 ppmw $Tb^{3+}$: Ge–As–Ga–Se bulk glasses. The upper transition state is identified in each case.

It is well known that the accuracy of J–O modeling is critically dependent on the accuracy of the absorption cross sections of the RE ion in the host concerned. That means the need to know the area under exclusively the RE electronic absorption bands in the absorption spectrum of the RE-doped host. However, here, in the case of $Tb^{3+}$-doped Ge–As–Ga–Se glasses, we know that the $^7F_6 \rightarrow {}^7F_5$ and $^7F_6 \rightarrow {}^7F_4$ transitions overlie and obscure from view the vibrational absorption due to -[O–H] and [H–Se]- contamination, respectively. Furthermore, it is known that the extrinsic vibrational absorption cross sections are greater in the case of the $Tb^{3+}$-doped chalcogenide glasses than in the undoped chalcogenide host glass with no Tb present because the Tb precursor chemical brings added anionic impurities into the glass. The manufacturer's stated purity of the Tb precursor is 4 × 9 s, but this refers exclusively to cationic not anionic impurities. Therefore, it was imperative here to separate out the true contribution of electronic absorption due solely to $Tb^{3+}$ from the observed absorption spectrum of the $Tb^{3+}$-doped selenide-chalcogenide glass, which incorporated not only electronic absorption due solely to $Tb^{3+}$ but also vibrational extrinsic absorption bands due to unwanted anionic impurities in the glass host matrix. To obtain the true $Tb^{3+}$-absorption cross section, we followed the detailed method presented in [8], which is described below.

Step 1. The absorption spectrum of the $Tb^{3+}$-doped Ge–As–Ga–Se glass was collected.
Step 2. The $Tb^{3+}$ electronic absorption bands were identified.
Step 3. Known anionic impurities in chalcogenide glasses were considered, and one absorption band of one impurity was selected for analysis—for the sake of argument, here the impurity [H–Se]- vibrational absorption band centered at 4.6 μm wavelength was selected.
Step 4. The absorption spectrum of $Dy^{3+}$-doped Ge–As–Ga–Se glass was collected as $Dy^{3+}$ has no electronic ground-state absorption at around 4.6 μm wavelength.
Step 5. Gaussian bands were fixed in ratio to fix the band shape of the [H–Se]- absorption centered around 4.6 μm wavelength in the absorption spectrum collected for $Dy^{3+}$-doped Ge–As–Ga–Se glass in Step 4.
Step 6. The entire combined absorption band of {$Tb^{3+}$ + [H–Se]–} in the 3.0–5.5 μm wavelength region of the absorption spectrum of the $Tb^{3+}$-doped Ge–As–Ga–Se bulk glass was Gaussian fitted using (i) the fixed ratio for [H–Se]– (found in Step 5) and allowing the H–Se– bands to vary in intensity but remain in fixed ratio to each other and (ii) the minimum of other Gaussian bands to optimize the fitting to the combined absorption band of {$Tb^{3+}$ + [H–Se]–}.

Step 7. The observed absorption coefficient band shape of the combined {$Tb^{3+}$ + [H–Se]–} absorption band was then deconvoluted into its component parts of [H–Se]- vibrational absorption and the true $Tb^{3+}$ absorption cross section.
Step 8. Steps 1–7 were repeated for the impurity –[O–H] vibrational absorption band centered close to 2.95 μm wavelength.

In this way, the true absorption cross sections of the $Tb^{3+}$ ground-state transitions $^7F_6 \rightarrow {}^7F_4$ and $^7F_6 \rightarrow {}^7F_5$ were calculated [see Figs. 4(a) and 4(b)].

The calculated absorption and emission cross sections for $Tb^{3+}$-doped 1000 ppmw Ge–As–Ga–Se chalcogenide glass are presented in Fig. 5. The absorption cross sections ($\sigma_{abs}$) were directly obtained from the corrected absorption spectrum using the following formula:

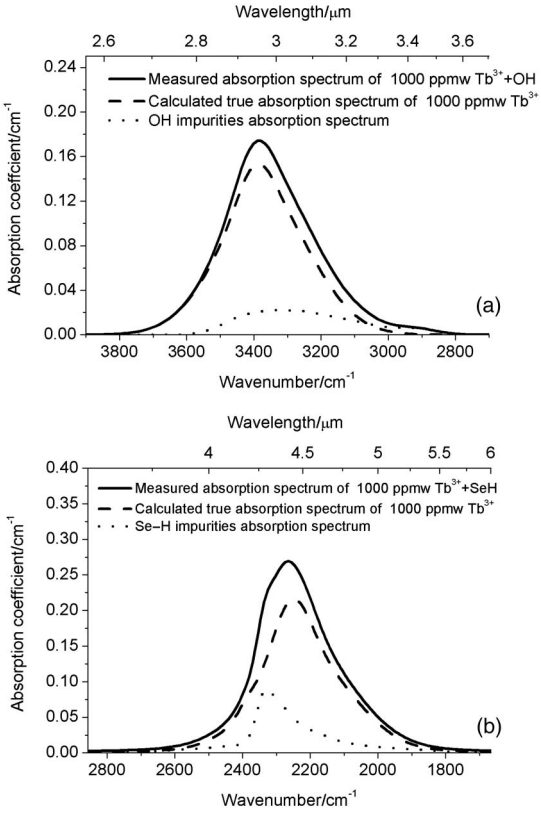


**Fig. 4.** (a) Absorption spectrum of the $^7F_6 \rightarrow {}^7F_4$ transition in 1000 ppmw $Tb^{3+}$-doped Ge–As–Ga–Se bulk glass. The solid line indicates the measured absorption spectrum of the $^7F_6 \rightarrow {}^7F_4$ transition, which is comprised of both the $Tb^{3+}$ absorption and the OH impurity absorption bands. The dashed line represents the true absorption spectrum of the $^7F_6 \rightarrow {}^7F_4$ transition after calculation to remove the OH contribution. The dotted line represents the calculated contribution of the OH impurity to absorption in the 1000 ppmw $Tb^{3+}$-doped Ge–As–Ga–Se bulk glass. (b) Absorption spectrum for the $^7F_6 \rightarrow {}^7F_5$ transition of 1000 ppmw $Tb^{3+}$-doped Ge–As–Ga–Se bulk glass. The solid line indicates the measured absorption spectrum of the $^7F_6 \rightarrow {}^7F_5$ transition, which is comprised of both the $Tb^{3+}$ absorption and the Se–H impurity absorption bands. The dashed line represents the true absorption spectrum of the $^7F_6 \rightarrow {}^7F_5$ transition after calculation to remove the Se–H contribution. The dotted line represents the calculated contribution of the Se–H impurity to absorption in the 1000 ppmw $Tb^{3+}$-doped Ge–As–Ga–Se bulk glass.

$$\sigma_{abs} = \frac{\alpha(\lambda)}{N}, \tag{2}$$

where $N$ is $Tb^{3+}$ the ion density equal to $1.65 \times 10^{25}$ ions/$m^3$, which corresponds to 1000 ppmw $Tb^{3+}$-doped glass Ge–As–Ga–Se, and $\alpha(\lambda)$ is the absorption coefficient of the 1000 ppmw $Tb^{3+}$-doped glass Ge–As–Ga–Se.

The emission cross sections ($\sigma_{em}$) were calculated from the corrected observed absorption spectra using the McCumber method. In this case, we derived the emission cross section from a corrected observed absorption spectrum instead of using the measured photoluminescence spectrum, whose shape may be affected by the Se–H impurity band [8].

The emission cross section of the $^7F_5 \rightarrow {}^7F_6$ transition was scaled using [14]

$$\sigma_{em} = \frac{\lambda^4}{8\pi n^2 c} A_{jj'r} \Delta\lambda, \tag{3}$$

where $\Delta\lambda = I(\lambda)/\int I(\lambda)d\lambda$ is the line shape of the emission band, and $I(\lambda)$ is the emission intensity from $^7F_5 \rightarrow {}^7F_6$, $n$ is the refractive index ($n \approx 2.53$) (see Fig. 1), $c$ is the speed of light in the vacuum, $A_{jj'r}$ is the spontaneous emission rate of the $^7F_5 \rightarrow {}^7F_6$ transition (taken from Table 1), and $\lambda$ is the central wavelength of the emission (4.7 μm) [14]. The emission cross section of the transition value from $^7F_5$ to the ground state here was calculated to be $0.94 \times 10^{-24}$ $m^2$ at 4.7 μm.

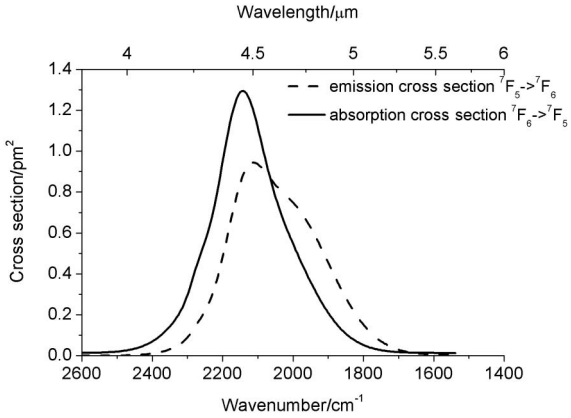


**Fig. 5.** Absorption cross section for the $^7F_6 \rightarrow {}^7F_5$ transition (solid curve, measured but with removal of the contribution of the Se–H impurity band). Emission cross section for the transition $^7F_5 \rightarrow {}^7F_6$ (dashed curve, calculated using McCumber theory from the corrected absorption cross section). The absorption cross section was calculated for 1000 ppmw $Tb^{3+}$-doped Ge–As–Ga–Se bulk glass.

**Table 1. Calculated Spontaneous Emission Rates [Electronic ($A_{ED}$) and Magnetic ($A_{MD}$)], Radiative Branching Ratios ($\beta_{rad}$), and Radiative Lifetimes ($\tau_{rad}$) for Emissions Observed Centered at Wavelength $\lambda$**

| Transition ($J \rightarrow J'$) | $\lambda/(\mu m)$ | $A_{ED}/(s^{-1})$ | $A_{MD}/(s^{-1})$ | $\beta_{rad}$ | $\tau_{rad}/(ms)$ |
|---|---|---|---|---|---|
| $^7F_5 \rightarrow {}^7F_6$ | 4.8 | 70.78 | 5.77 | 1 | 13.1 |
| $^7F_4 \rightarrow {}^7F_5$ | 7.9 | 16.11 | 2.8 | 0.10 | 5.8 |
| $^7F_4 \rightarrow {}^7F_6$ | 3.0 | 153.31 | | 0.90 | 5.8 |

This value is in good agreement with emission cross sections reported in the literature for other selenide-chalcogenide glasses [5]. The calculated emission cross section shows a maximum at a wavelength of 4.7 μm for the bulk glass sample, where the mid-infrared emission full width at half-maximum bandwidth is equal to 0.850 μm.

### C. Judd–Ofelt Modeling

Using the true absorption cross sections of $Tb^{3+}$ in the $Tb^{3+}$-doped Ge–As–Ga–Se glass, the emission cross sections derived from the true absorption cross sections and the measured refractive index of the $Tb^{3+}$-doped Ge–As–Ga–Se glasses, the J–O parameters for this system were calculated as $\Omega_2 = (6.43 \pm 1.3) \times 10^{-20}$ cm$^2$, $\Omega_4 = (3.50 \pm 0.7) \times 10^{-20}$ cm$^2$, and $\Omega_6 = (2.92 \pm 0.58) \times 10^{-20}$ cm$^2$, and radiative rates, lifetimes, and branching ratios were calculated (Table 1).

The relative errors of J–O analysis can be as high as 30%–35% [15,16]. These errors result from the uncertainty, which is inherent to the determination of the integral absorption coefficients, error in estimation of $Tb^{3+}$ concentration, and the accuracy of the refractive index measurement. The errors also depend on the accuracy with which the influence of impurities in the matrix host on the absorption cross section can be extracted. Therefore, radiative rates, the branching ratio, and absorption and emission cross sections are estimated with ±35% error.

Figure 6 shows the normalized decay of the luminescent intensity at 4.7 μm under 2.013 μm excitation, fitted most simply to a single exponential with time constant $\tau_m = 12.9$ ms. Reasonable agreement was found between the measured ($\tau_m = 12.9$ ms) and calculated lifetime ($\tau_{\text{rad}} = 13.1$ ms, Table 1) for the $^7F_5$ radiative transition to ground state $^7F_6$. If nonradiative decay solely due to intrinsic multiphonons alone is considered, then as the glass highest phonon energy is ~300 cm$^{-1}$, the observed 4.7 μm emission should be mainly radiative, with a quantum efficiency close to 98.47%. We have

$$\eta = \frac{\tau_m}{\tau_{\text{rad}}}, \tag{4}$$

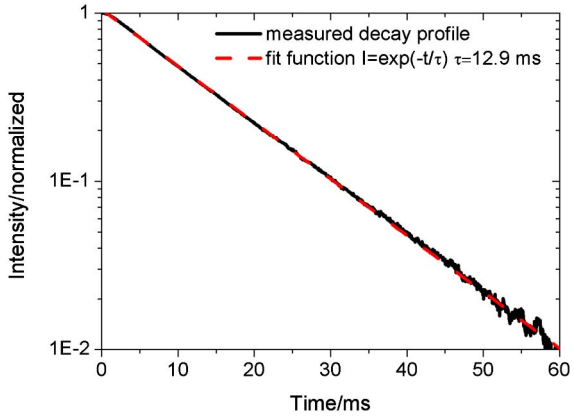


**Fig. 6.** Decay time of the $^7F_5$ excited level of 1000 ppmw $Tb^{3+}$-doped chalcogenide selenide glass bulk sample measured at 4.7 μm after QCW (6–8 Hz) laser excitation at 2.013 μm. The best fit to the measured decay profile yields a single exponential decay with $\tau_m = 12.9$ ms.

where $\tau_m$ is a measured lifetime for the $^7F_5 \rightarrow {}^7F_6$ transition (see Fig. 6) and $\tau_{\text{rad}}$ is a radiative lifetime calculated from J–O theory for the $^7F_5 \rightarrow {}^7F_6$ transition (see Table 1).

However, we suggest that there is a population of $Tb^{3+}$ ions in the host matrix that is sited adjacent to [H–Se]- impurity, leading to resonant depopulation of the excited state of high probability and giving low quantum efficiency and radiative energy loss to heat [1]. Note that Churbanov *et al.* [17] found that the decay time of the $^7F_5$ state of $Tb^{3+}$-doped selenide-iodide chalcogenide glasses decreased with increasing (inferred) [H–Se]- contamination. A long decay time of $\tau_m = 16.1$ ms was observed for the purest (considering only [H–Se]- impurity bonds) sample.

Emission at 3.0 μm due to the $^7F_4 \rightarrow {}^7F_6$ transition was not experimentally observed. We tentatively propose that this $^7F_4$ manifold is depopulated in a nonradiative way. The energy gap (1265 cm$^{-1}$) of the $^7F_4 \rightarrow {}^7F_5$ transition may be bridged effectively by only four host glass phonons. However, in addition, the $^7F_4 \rightarrow {}^7F_5$ transition may be depopulated by the nonradiative transfer of energy to extrinsic molecular water ($H_2O$) impurities in the selenide-chalcogenide glass matrix with vibrational absorption at 6.3 μm (H–O–H bending), which has a first overtone at ~3 μm that is resonant with the $^7F_4 \rightarrow {}^7F_6$ transition at ~3 μm. Hence, from arguments found in [1], quenching of the $^7F_4 \rightarrow {}^7F_5$ transition in $Tb^{3+}$-doped Ge–As–Ga–Se glass due to nonradiative decay and concurrent stimulation of H–O–H bending vibration is expected to occur. Note that quenching of the $^7F_4 \rightarrow {}^7F_6$ transition at ~3 μm was also reported in [5], where the measured lifetime from $^7F_4 \rightarrow {}^7F_5$ was approximately equal to 12 μs. Therefore, we propose that the $^7F_3$, $^7F_2$, $^7F_1$, and $^7F_0$ upper levels are depopulated nonradiatively (see Fig. 2). This result suggests that terbium (III) operating at 4.7 μm and pumped at 2.95 μm could operate as a three-level laser system like that of the erbium- (III) doped silica glass fiber amplifier operating at 1.55 μm when pumped at 0.98 μm [14].

The emission cross section and lifetime of the $^7F_5 \rightarrow {}^7F_6$ transition (see Fig. 5) are in reasonable agreement with values for $Tb^{3+}$-doped selenide-chalcogenide glass in [5].

$\sigma_{\text{em}} \times \tau_m$ characterizes gain in RE-doped materials. For the $^7F_5 \rightarrow {}^7F_6$ transition in the $Tb^{3+}$-doped Ge–As–Ga–Se glasses here, $\sigma_{\text{em}} \times \tau_m = 12.1 \times 10^{-24}$ m$^2$ ms and is, for instance, two orders of magnitude larger than in gallium lanthanum sulfide-oxide [GLS(O)] bulk glass [18] and is greater than in crystalline $KPb_2Br_5$ [19] (Table 2). A long decay lifetime for the $KPb_2Br_5$ crystal is a direct consequence of the low phonon energy of this material of ~140 cm$^{-1}$.

500 ppmw $Tb^{3+}$-doped Ge–As–Ga–Se unstructured fiber and 1000 ppmw $Tb^{3+}$-doped Ge–As–Ga–Se bulk glass when pumped at 2.013 μm into the $^7F_2$ level gave emission across ~4.1–5.9 μm (Fig. 7). Photoluminescence was collected from the fiber end opposite to the pump end. The fibers used in the experiment were ~350 μm diameter and were 65 mm length. The host in each case was the selenide glass Ge–As–Ga–Se. This emission is attributed to the $Tb^{3+}$ $^7F_5 \rightarrow {}^7F_6$ transition, and the difference in band shape between the bulk glass and the fiber is attributed to photon migration [11], with the longer path length fiber causing band shape distortion.

**Table 2. Measured Luminescent Lifetimes ($\tau_m$), Emission Cross Section ($\sigma_{em}$), and Product of Merit ($\sigma_{em} \times \tau_m$) of $^7F_5 \rightarrow {}^7F_6$ in $Tb^{3+}$-Doped Mid-Infrared Optical Materials**

| $Tb^{3+}$ in Glass or Crystal Host | $\tau_m$/ms | $\sigma_{em}$ (at 4.7 μm)× $10^{-24}$/m$^2$ | $\sigma_{em} \times \tau_m$× $10^{-24}$/m$^2$ ms |
|---|---|---|---|
| Ge–As–Se–Ga glass (1000 ppmw)[a] | 12.9 | 0.94 | 12.12 |
| Ge–As–Se–Ga glass (1000 ppmw) [5] | 11.0 | 1.05 | 11.55 |
| GLS(O) glass (0.2 mol. %) [18] | 0.10 | 0.89 | 0.089 |
| $KPb_2Br_5$ crystal [19] | 22.0 | 0.40 | 8.80 |

[a]This work.

## 4. NONRADIATIVE DECAY IN RARE-EARTH-ION-DOPED SELENIDE GLASSES

### A. Intrinsic Multiphonon Depopulation of RE Excited States

The intrinsic phonon energy of the $Tb^{3+}$-doped Ge–As–Ga–Se glass is assumed to be 300 cm$^{-1}$ [1]. The probability of intrinsic multiphonon relaxation, $A_{MP}$, is [1,14]

$$A_{MP}(T) = B(n(T) + 1)^p \exp(-\alpha \Delta E), \quad (5)$$

where $T$ is assumed as 300 K, $\alpha$ and $B$ are experimentally determined parameters assumed constant for a given host glass and derived from fitting Eq. (5) to the experimentally determined $A_{MP}$ dependence against energy gap ($\Delta E$), and $p$ is the number of phonons required to bridge $\Delta E$:

$$p = \frac{\Delta E}{\hbar \omega}, \quad (6)$$

where $\hbar\omega$ is the intrinsic multiphonon energy. In Eq. (5), $n(T)$ is the Bose–Einstein number, which describes the phonon population as a function of temperature ($T$):

$$n(T) = \frac{1}{\exp(\hbar\omega/kT) - 1}. \quad (7)$$

At low RE concentration levels and short path lengths, RE ion–ion interactions may be ignored and ideally the intrinsic multiphonon relaxation rate transition probability may be assumed equal to the nonradiative relaxation rate. The intrinsic multiphonon relaxation rate increases exponentially with the decrease in energy gap, $\Delta E$, which must be bridged by the phonons. We have

$$A_{MP} = A_T - A_R, \quad (8)$$

where $A_T$ is the observed excited state decay rate, and $A_R$ is the radiative rate calculated from J–O theory. In this work, we used data from [5,20] to fit the $A_{MP}$ dependence on the energy gap (Fig. 8) giving $\alpha = 0.0074$ cm$^{-1}$ and $B = 6.82 \times 10^7$ s$^{-1}$ for the Ge–As–Ga–Se glass host. Selenide-chalcogenide glasses exhibit their lowest nonradiative rates within the 3 μm (3333 cm$^{-1}$) to 6 μm (1666 cm$^{-1}$) wavelength range. Emission >1265 cm$^{-1}$ ($\lesssim$ 8 μm) is denied, supporting the proposal (Section 3) that the $^7F_4$ level in $Tb^{3+}$-doped Ge–As–Ga–Se glass is depopulated nonradiatively.

Comparison between nonradiative rates for various optical fiber glass can be found in [21].

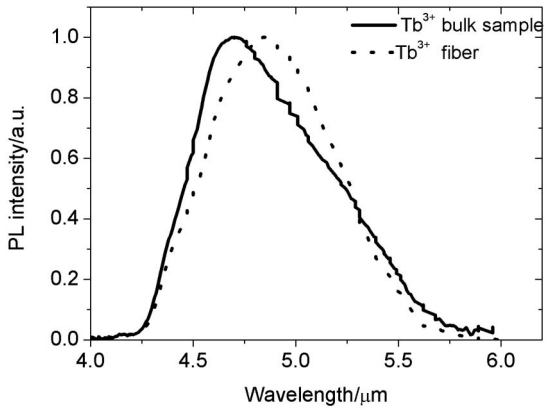


**Fig. 7.** Measured MIR emission spectra of 1000 ppmw $Tb^{3+}$: bulk sample and 500 ppmw $Tb^{3+}$ glass fiber under excitation at 2.013 μm; spectra are normalized to 1. The emission intensities were corrected for the system response.

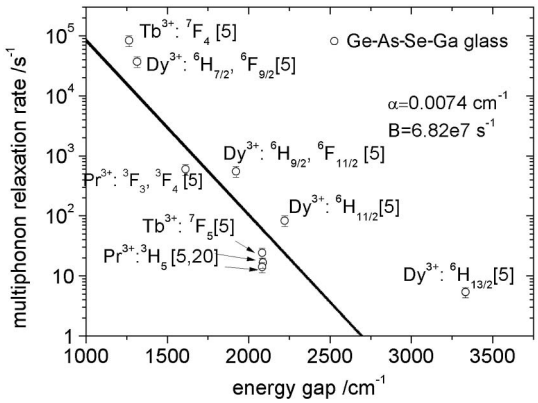


**Fig. 8.** Calculated dependence of the multiphonon relaxation rate on the energy gap for selenide-chalcogenide optical bulk glasses based on Ge–As–Ga–Se calculated based on the data presented in [5,20]. The black line indicates the best fit to calculated intrinsic multiphonon relaxation rates in rare-earth-doped selenide-chalcogenide glasses.

### B. Intrinsic Multiphonon Depopulation of RE Excited States Versus Extrinsic Resonant and Overtone Depopulation of RE Excited States

Assuming that the maximum intrinsic phonon energy of $Tb^{3+}$-doped Ge–As–Ga–Se is ~300 cm$^{-1}$ [1], the emission transition $^7F_4 \rightarrow {}^7F_5$, which has an energy gap of transition of ~1265 cm$^{-1}$ (7.91 μm), is predicted to be depopulated fast and nonradiatively as the transition may be bridged by ~4 host intrinsic phonons. On the other hand, impurity ≡Ge–O- in the glass has vibrational absorption at ~8 μm [1] and so resonant nonradiative emission via extrinsic vibrational photon-assisted depopulation is also possible [1]. $Tb^{3+}$ electronic transitions from the upper levels $^7F_3$, $^7F_2$, $^7F_1$, and $^7F_0$ levels are expected to be host phonon assisted and resonant and overtone vibrational photon absorption from the electronic state can occur.

As stated in [1], in impure glasses it is more correct to count the $Tb^{3+}$ population in the glass as composed of subpopulations where the ideal subpopulation is exposed only to the

possibility of intrinsic multiphonon decay and then for the $^7F_5 \rightarrow {}^7F_6$ transition radiative decay and lasing is possible. Nonideal subpopulations of the doped-in $Tb^{3+}$ may be adjacent to oxide (such as =[As–O]-) with broadband fundamental absorption centered at 12 μm [13] and hydride (such as [H–Se]-) with broad fundamental absorption centered at 4.6 μm. Resonant nonradiative decay due to extrinsic vibrational absorption of the long-lived excited state $^7F_5 \rightarrow {}^7F_6$ is very probable for the subpopulation of $Tb^{3+}$ ions adjacent to [H–Se]-. Multiphoton (i.e., overtone absorption) nonradiative decay due to extrinsic vibrational absorption of the long-lived excited state $^7F_5 \rightarrow {}^7F_6$ is quite probable for the subpopulation of $Tb^{3+}$ ions adjacent to =[As–O]-. However, it is possible that the probability of nonradiative decay of the $Tb^{3+}$ excited state decreases much more rapidly as the number of photons required to bridge the gap of the potentially radiative RE transition in extrinsically mediated multiphoton nonradiative decay than in intrinsically mediated multiphonon decay.

## 5. POPULATION INVERSION IN $Tb^{3+}$ CHALCOGENIDE GLASS AND FIBER

Rate equations were employed here mimic the erbium-doped fiber amplifier operating as a continuous wave (CW) at 1.55 μm and pumped at 0.98 μm [14]:

$$\frac{dN_3}{dt} = W_{pa}N_1 - (W_{pe} + W_{31} + W_{32})N_3, \tag{9}$$

$$\frac{dN_2}{dt} = W_{sa}N_1 - (W_{se} + W_{21})N_2 + W_{32}N_3, \tag{10}$$

$$N = N_1 + N_2 + N_3, \tag{11}$$

where $N_i$, $i = 1$, 2, and 3, are the ion population of energy levels 1, 2, and 3, respectively, and $W_{xy}$ are the transition rates between levels $x$ and $y$. The transition rates are defined as follows: the absorption and emission rates $W_{pa}$, $W_{pe}$, $W_{sa}$, and $W_{se}$ of the pump and signal, respectively.

In the steady state $\left(\frac{dN_i}{dt} = 0\right)$, Eqs. (9)–(11) reduce to three algebraic equations.

In Eqs. (9)–(11), the stimulated emission or absorption rates are expressed by

**Table 3. $Tb^{3+}$-Doped Selenide-Chalcogenide Glass Fiber Laser Modeling Parameters**

| Quantity | Parameter | Value | Unit |
|---|---|---|---|
| Ion concentration | $N$ | $8.25 \times 10^{24}$ | ions/m$^3$ |
| Fiber length | $L$ | 0.1–3 | m |
| Fiber core diameter | $D_{core}$ | 30 | μm |
| Fiber numerical aperture | NA | 0.4 | — |
| Confinement factor for pump wavelength at 2.013/2.95 μm | $\Gamma_p$ | 0.9 | — |
| Confinement factor for signal wavelength at 4.7 μm | $\Gamma_s$ | 0.9 | — |
| Pump absorption cross section at 2.013/2.95 μm | $\sigma_{pa}$ | $0.73 \times 10^{-24}$<br>$0.92 \times 10^{-24}$ | m$^2$ |
| Pump emission cross section at 2.013/2.95 μm | $\sigma_{pe}$ | $0.7 \times 10^{-24}$<br>$0.85 \times 10^{-24}$ | m$^2$ |
| Lifetime of level $^7F_4$ | $\tau_{32}$ | 0.012 | ms |
| Lifetime of level $^7F_5$ | $\tau_{21}$ | 12.9 | ms |

$$W_{xy} = \frac{\Gamma_x \sigma_{xy} \lambda_x P_x}{Ahc}, \tag{12}$$

where $\Gamma_x$ is the confinement factor, which defines the fraction of energy that propagates in the core to the total energy that propagates in the fiber (core and the clad) [14], $\sigma_{xy}$ is the absorption or emission cross section for the $x$–$y$ transition, $P_x$ denotes the propagating signal and pump powers, respectively, $A$ is the doping cross-section area, $h$ is Planck's constant, $\lambda_x$ is the wavelength of signal or pump, and $c$ is the speed of light in free space.

Total decay rates $W_{ij}$ are calculated by

$$W_{ij} = W_{ij}^{r} + W_{ij}^{mp} + W_{ij}^{imp}, \tag{13}$$

where $W_{ij}^{r}$ and $W_{ij}^{mp}$ are radiative and host multiphonon decay rates from the level $i$ to the level $j$, respectively, taken from Table 1 and Fig. 8. Note that $W_{ij}^{imp}$ was defined in [1] as the decay rate due to impurity resonant and multiphoton depopulation of the excited state. This is an integral across many different vibrational absorption energies and extinction coefficients and represents the real situation; here this was ignored and the ideal situation was modeled.

The forward $P_x^+$ and reverse $P_x^-$ propagation of pump $P_p$ and signal $P_s$ powers along the active fiber are described by the following differential equations:

$$\frac{dP_p^{\pm}}{dz} = \pm\Gamma_p(\sigma_{pe}N_3 - \sigma_{pa}N_1)P_p^{\pm} \mp \alpha_p P_p^{\pm}, \tag{14}$$

$$\frac{dP_s^{\pm}}{dz} = \pm\Gamma_s(\sigma_{21e}N_2 - \sigma_{21a}N_1)P_s^{\pm} \mp \alpha_s P_s^{\pm}, \tag{15}$$

where "+" and "–" refer to forward and backward traveling waves, respectively, $P_p^{\pm} = P_p^{+} + P_p^{-}$, and $P_s^{\pm} = P_s^{+} + P_s^{-}$.

$\sigma_{pa}$, $\sigma_{pe}$, $\sigma_{21a}$, and $\sigma_{21e}$ are the absorption and emission cross sections of the pump and signal, respectively. To find output power, the photon fluxes are integrated back/forth, subject to reflective boundary conditions imposed at each fiber end and repeated to get convergence of the photon flux (detailed in [7,14]), using the experimentally determined excited-state lifetimes of 12.9 ms for the $^7F_5$ level (see Fig. 6) and 12 μs for the $^7F_4$ level ([5]). The $Tb^{3+}$ ion density in the Ge–As–Ga–Se host was $8.25 \times 10^{24}$ ions/m$^3$ (= 500 ppmw). Table 3 lists the modeling parameters.

Figure 9 shows the calculated material gain (in 1/m) as a function of the pump intensity for a Ge–As–Ga–Se glass doped with $Tb^{3+}$ at a level of 500 ppmw ($8.25 \times 10^{24}$ ions/m$^3$) obtained by numerical solution of the steady state rate equations [Eqs. (9)–(13)] for pumping at 2.013 μm and 2.95 μm, respectively, and assuming nonradiative emission solely via the selenide-chalcogenide glass host intrinsic phonons.

The material gain was obtained using the relation

$$\Delta N = \sigma_{em}N_2 - \sigma_{abs}N_1, \tag{16}$$

where $N_2$ and $N_1$ are the populations of the $^7F_5$ and $^7F_6$ levels, respectively, and $\sigma_{abs}$ and $\sigma_{em}$ are the absorption and emission cross sections at 4.7 μm, respectively (Fig. 5). From Fig. 9, positive gain was found for $^7F_5 \rightarrow {}^7F_6$ pumping at either 2.013 or 2.95 μm. The pump intensity necessary to render $Tb^{3+}$-doped material transparent was determined to be 20 MW/m$^2$ and 10.7 MW/m$^2$ for a 2.013 μm pump and 2.95 μm pump, respectively. A high gain at 4.7 μm would help

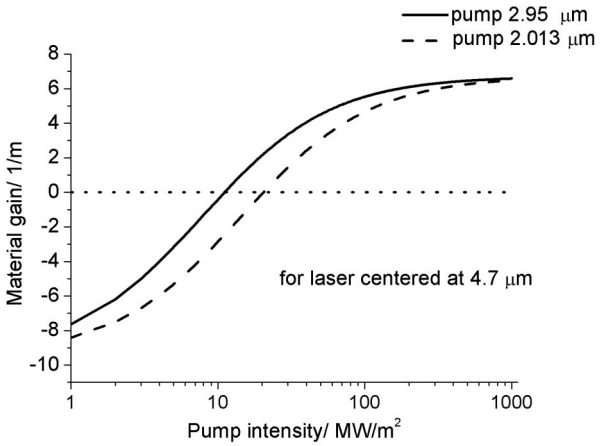


**Fig. 9.** Calculated material gain $\Delta N = \sigma_{em}N_2 - \sigma_{abs}N_1$ as a function of the pump intensity for different pumping wavelengths and for laser emission at 4.7 μm in $Tb^{3+}$-doped Ge–As–Ga–Se.

reduce the active fiber length required to achieve efficient laser action at 4.7 μm. The experimentally estimated power damage threshold for selenide glass fiber has been reported to be ~250 MW/m$^2$ [22]. On the other hand, it has also been shown that the power damage threshold can be significantly increased by operation in a quasi-continuous wave (QCW) regime [23].

For modeling the performance of a 500 ppmw ($8.25 \times 10^{24}$ ions/m$^3$) $Tb^{3+}$-doped Ge–As–Ga–Se fiber lasing in the $^7F_5 \rightarrow {}^7F_6$ transition, a SIF structure was assumed, with core diameter = 30 μm, NA = 0.4 [2], loss <1 dBm$^{-1}$ at all considered wavelengths [4], and fiber Bragg gratings (FBGs) to control the cavity with reflectivity at the fiber-input FBG at pump and signal wavelengths of 0.05 and 0.95, respectively, and fiber-output FBG reflectivity at pump and signal wavelengths of 0.9 and 0.05, respectively. A fiber with a similar structure has already been reported in the literature by our group [2]. In this paper [2], we have shown that the spectroscopic properties achieved for a bulk sample are also sustained for a small-core step index fiber. Fiber-laser performance was analyzed using self-consistent numerical solution of the rate and propagation equations [Eqs. (9)–(16)].

Dependence of output power on the cavity length was assessed by a systematic increase of loss [Fig. 10(a)] for pump power = 1 W and lasing and pump wavelengths of arbitrarily 4.7 μm and 2.95 μm, respectively. Maximum output power was 0.42 W for a 0.9 m cavity length and 1 dB/m fiber loss. For fiber loss fixed at 3 dB/m, the maximum output power was reduced to a maximum 0.26 W for a fiber length of 0.8 m. Rapid increase of the output power was observed with an increase in cavity length, reaching a maximum at 0.8 m and decreasing with increasing cavity length. This behavior is attributed to signal reabsorption, attenuation, and pump-power depletion. Figure 10(b) shows threshold pump power as a function of cavity length (fiber loss). The minimum threshold was 25 mW and 35 mW for 1 dB/m and 3 dB/m loss, respectively. Figure 10 indicates that fiber lasing is achievable in a three-level system rather than previously designed cascading systems reliant on multiple FBGs to offset long-lived levels leading to termination [4,24].

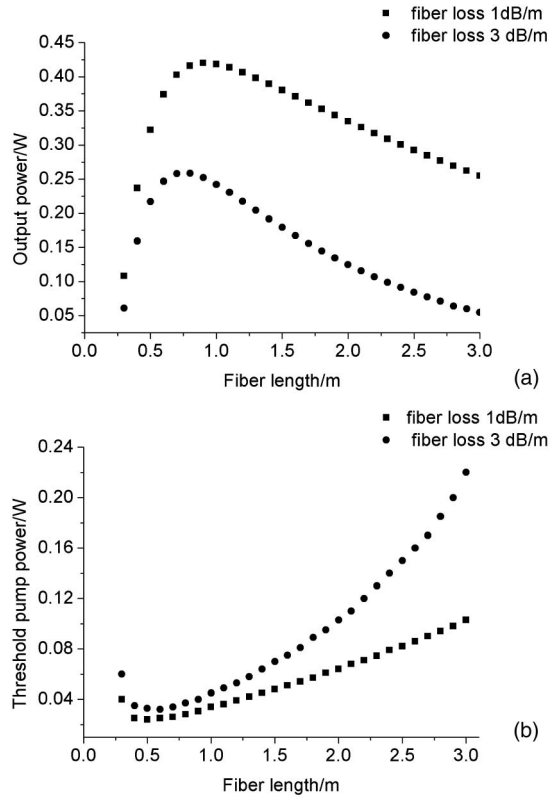


**Fig. 10.** (a) Calculated laser power ($\lambda_s$ = 4.7 μm) and (b) threshold pump powers as a function of fiber length with different levels of fiber background loss. The results were achieved with an input pump power $P_p$ = 1 W and pump wavelength set at 2.95 μm. Results are plotted for a fiber with a background loss of 1 dB/m and 3 dB/m.

To investigate the influence of output coupling on fiber lasing, output power was plotted as a function of cavity length for different values of output coupler reflectance, $R$ (Fig. 11). Figure 11 indicates that the maximum possible output power was reduced, and the position of maximum output power shifted to shorter length, for an increase in $R$, attributed to lower cavity loss at higher $R$ and shorter fiber length needed for maximum output power.

Figure 12 shows output power as a function of lasing wavelength, for two loss levels, for the pump wavelength and fiber length fixed at 2.95 μm and 0.9 m, respectively, and pump power = 1 W. The results suggest that a $Tb^{3+}$-doped Ge–As–Ga–Se fiber laser could efficiently lase within the range of 4.5–5.3 μm.

Investigating the output power dependence on pump wavelength in the range of 2.75–3.2 μm (Fig. 13), this pump wavelength region is provided with several, e.g., Er:YAG, solid-state lasers and semiconductor ICLs [25]. We define the optimum fiber length as the fiber length for which maximum output power occurs. The pump power and fiber background loss were set to 1 W and 1 dB/m, respectively. From Fig. 13, output power increases steeply with increasing pump wavelength, achieves a maximum of 0.42 W at 2.95 μm, and then decreases with further increase in pump wavelength. Also, the optimum fiber length rapidly decreases with an initial increase in the

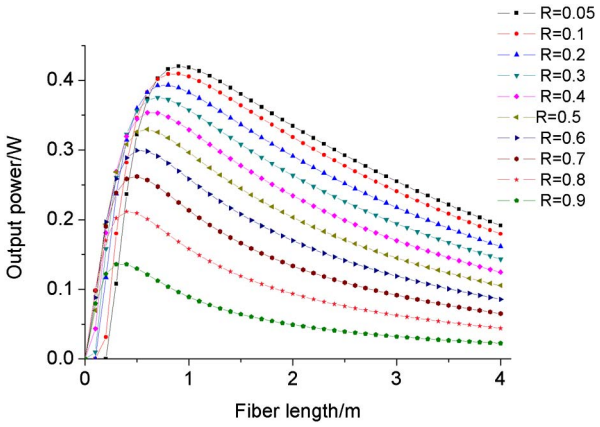


**Fig. 11.** Calculated laser power ($\lambda_s = 4.7$ μm) as a function of fiber length for different values of reflectivity of the output coupler. The results were achieved with an input pump power $P_p = 1$ W and a pump wavelength set to 2.95 μm. Results are plotted for a fiber with a background loss of 1 dB/m.

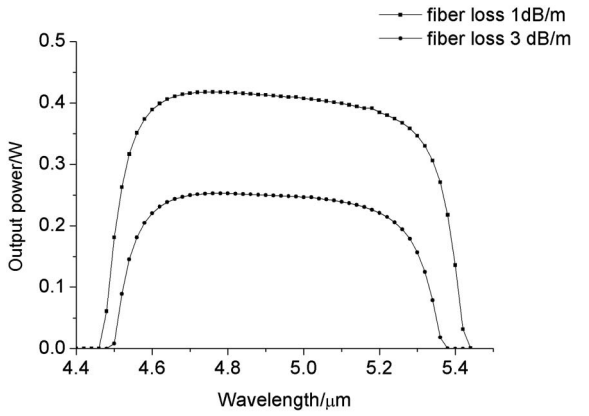


**Fig. 12.** Calculated output power as a function of lasing wavelength at a pump power of 1 W. The pump wavelength and fiber length are fixed at 2.95 μm and 0.9 m, respectively. Results are plotted for a fiber with a background loss of 1 dB/m and 3 dB/m, respectively.

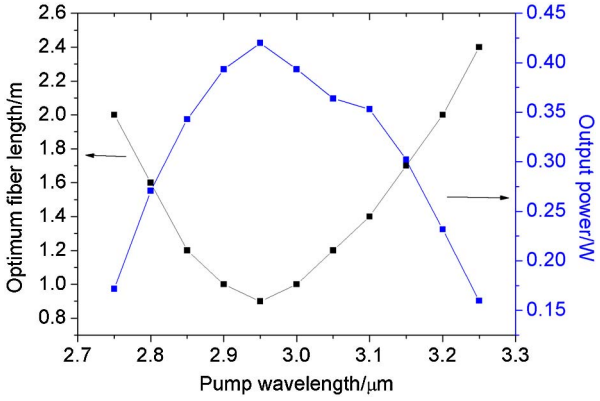


**Fig. 13.** Calculated output power and optimum fiber length as a function of pumping wavelength. Results are plotted for a fiber with a background loss of 1 dB/m.

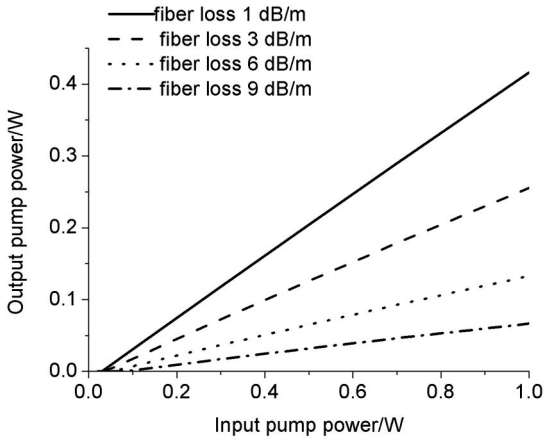


**Fig. 14.** Calculated output power as a function of input pump power for different fiber background losses. Results were calculated for the signal wavelength and the pump wavelength set to 4.7 μm and 2.95 μm, respectively.

pump wavelength, reaching a minimum of 0.9 m for a pump wavelength of 2.95 μm and then increasing as pump wavelength is further increased. That the output power and optimum fiber length reach their respective maximum and minimum values at a pump wavelength of 2.95 μm is due to the maximum in absorption cross section at this wavelength [see Fig. 4(a)]. High values of pump absorption cross section ensure that pump power is more quickly absorbed, which results in a shorter fiber length and correspondingly smaller attenuation loss. Based on the results presented above, it can be concluded that the pump wavelength and fiber length should be optimized simultaneously in order to achieve the best laser performance.

To estimate the effect of fiber loss on fiber-laser operation, the output power was calculated as a function of input pump power for different values of fiber loss (Fig. 14). From Fig. 14, it can be seen that output-power and pump-power thresholds decrease and then increase gradually, from 0.42 W to 0.06 W and from 0.031 W to 0.08 W, respectively, as fiber loss increased from 1 to 9 dB/m. Naturally, to achieve MIR fiber lasing, good glass quality is key. Recently, our group has shown that in undoped Ge–As–Se fiber, background loss and loss due to the Se–H impurity vibration band absorption can be reduced to 0.1 dB/m and 1.6 dB/m, respectively [26].

## 6. CONCLUSIONS

We have demonstrated that quasi-three-level fiber lasing is feasible in $Tb^{3+}$-doped Ge–As–Ga–Se glass, giving low optical loss of $<1$ $dBm^{-1}$ at all wavelengths of interest in the fiber. We observe strong MIR emission in the range of 4.3–6.0 μm and a lifetime of 12.9 ms for the $^7F_5 \rightarrow {}^7F_6$ transition in Ge–As–Ga–Se bulk glass samples and fiber samples made in-house, *viz.*, bulk glasses doped with 500, 1000, and 1500 ppmw $Tb^{3+}$ and an unstructured optical fiber doped with 500 ppmw $Tb^{3+}$. The $^7F_4 \rightarrow {}^7F_6$ transition was not observed to emit radiatively at 3 μm wavelength, which is why $Tb^{3+}$-doped Ge–As–Ga–Se has the potential to act as a quasi-three-level

system laser; the upper pumping level $^7F_4$ is depopulated in a fast, nonradiative manner to $^7F_5$. We have modeled the fiber-laser performance and shown, using numerical modeling, that population inversion and gain within 4.5–5.3 μm may be achieved pumping at 2.013 or 2.95 μm. Laser action with 42% efficiency is projected for pumping at 2.95 μm.

**Funding.** Seventh Framework Programme (FP7) (317803); European Cooperation in Science and Technology (COST) (MP1401); Ministerstwo Nauki i Szkolnictwa Wyższego (MNiSW) (IP0441/IP2/2015/73); Engineering and Physical Sciences Research Council (EPSRC) (RDF/0312).

**Acknowledgment.** This research has been partly supported by the European Commission through the Seventh Framework Programme (FP7) project MINERVA (317803; http://minerva-project.eu) and by the EPSRC pump priming grant RDF/0312: Three level lasing host for mid-infrared (MIR) generation. The authors would like to acknowledge networking support from COST Action: MP1401. L. S. would like to acknowledge support by the Polish Ministry of Science and Higher Education under the project entitled "Iuventus Plus," 2016–2018 (IP0441/IP2/2015/73).

## REFERENCES

1. A. B. Seddon, Z. Tang, D. Furniss, S. Sujecki, and T. M. Benson, "Progress in rare-earth-doped mid-infrared fiber lasers," Opt. Express **18**, 26704–26719 (2010).
2. Z. Tang, D. Furniss, M. Fay, H. Sakr, L. Sójka, N. Neate, N. Weston, S. Sujecki, T. M. Benson, and A. B. Seddon, "Mid-infrared photoluminescence in small-core fiber of praseodymium-ion doped selenide-based chalcogenide glass," Opt. Mater. Express **5**, 870–886 (2015).
3. J. Schneider, "Fluoride fibre laser operating at 3.9 μm," Electron. Lett. **31**, 1250–1251 (1995).
4. R. S. Quimby, L. B. Shaw, J. S. Sanghera, and I. D. Aggarwal, "Modeling of cascade lasing in Dy:chalcogenide glass fiber laser with efficient output at 4.5 μm," IEEE Photon. Technol. Lett. **20**, 123–125 (2008).
5. L. B. Shaw, B. Cole, P. A. Thielen, J. S. Sanghera, and I. D. Aggarwal, "Mid-wave IR and long-wave IR laser potential of rare-earth doped chalcogenide glass fiber," IEEE J. Quantum Electron. **37**, 1127–1137 (2001).
6. Ł. Sójka, Z. Tang, H. Zhu, E. Bereś-Pawlik, D. Furniss, A. B. Seddon, T. M. Benson, and S. Sujecki, "Study of mid-infrared laser action in chalcogenide rare earth doped glass with $Dy^{3+}$, $Pr^{3+}$ and $Tb^{3+}$," Opt. Mater. Express **2**, 1632–1640 (2012).
7. S. Sujecki, A. Oladeji, A. Phillips, A. B. Seddon, T. M. Benson, H. Sakr, Z. Tang, E. Barney, D. Furniss, Ł. Sójka, E. Bereś-Pawlik, K. Scholle, S. Lamrini, and P. Furberg, "Theoretical study of population inversion in active doped MIR chalcogenide glass fibre lasers (invited)," Opt. Quantum Electron. **47**, 1389–1395 (2015).
8. A. B. Seddon, D. Furniss, Z. Q. Tang, Ł. Sojka, T. M. Benson, R. Caspary, and S. Sujecki, "True mid-infrared $Pr^{3+}$ absorption cross section in a selenide-chalcogenide host-glass," in *18th International Conference on Transparent Optical Networks (ICTON)* (IEEE, 2016), paper 7550709.
9. R. Swanepoel, "Determining refractive index and thickness of thin films from wavelength measurements only," J. Opt. Soc. Am. **2**, 1339–1343 (1985).
10. Y. Fang, L. Sojka, D. Jayasuriya, D. Furniss, Z. Q. Tang, C. Markos, S. Sujecki, A. B. Seddon, and T. M. Benson, "Characterising refractive index dispersion in chalcogenide glasses," in *Proceedings of 18th International Conference on Transparent Optical Networks* (IEEE, 2016), paper 7550618.
11. S. Kasap, "Influence of radiation trapping on spectra and measured lifetimes," in *The 7th International Conference on Optical, Optoelectronic and Photonic Materials and Applications (ICOOPMA)* (IEEE, 2016), paper 16263756.
12. J. S. Sanghera, V. Q. Nguyen, P. C. Pureza, R. E. Milos, F. H. Kung, and I. D. Aggarwal, "Fabrication of long lengths of low loss transmitting As40S(60-x)Sex glass fibers," J. Lightwave Technol. **14**, 743–748 (1996).
13. G. E. Snopatin, V. S. Shiryaev, V. G. Plotnichenko, E. M. Dianov, and M. F. Churbanov, "High-purity chalcogenide glasses for fiber optics," Inorg. Mater. **45**, 1439–1460 (2009).
14. P. C. Becker, N. A. Olsson, and J. R. Simpson, "Erbium-doped fiber amplifiers—amplifier basics," in *Erbium-Doped Fiber Amplifiers*, J. R. Simpson, ed. (Academic, 1999), pp. 131–152.
15. R. S. Quimby, N. J. Condon, S. P. O'Connor, and S. R. Bowman, "Excited state dynamics in Ho:$KPb_2Cl_5$," Opt. Mater. **34**, 1603–1609 (2012).
16. V. G. Truong, A. M. Jurdyc, B. Jacquier, B. S. Ham, A. Q. Le Quang, J. Leperson, V. Nazabal, and J. L. Adam, "Optical properties of thulium-doped chalcogenide glasses and the uncertainty of the calculated radiative lifetimes using the Judd–Ofelt approach," J. Opt. Soc. Am. B **23**, 2588–2596 (2006).
17. M. F. Churbanov, I. V. Scripachev, V. S. Shiryaev, V. G. Plotnichenko, S. V. Smetanin, E. B. Kryukova, Y. N. Pyrkov, and B. I. Galagan, "Chalcogenide glasses doped with Tb, Dy, and Pr ions," J. Non-Cryst. Solids **326**, 301–305 (2003).
18. T. Schweizer, B. N. Samson, J. R. Hector, W. S. Brocklesby, D. W. Hewak, and D. N. Payne, "Infrared emission and ion–ion interactions in thulium- and terbium-doped gallium lanthanum sulfide glass," J. Opt. Soc. Am. B **16**, 308–316 (1999).
19. K. Rademaker, W. F. Krupke, R. H. Page, S. A. Payne, K. Petermann, G. Huber, A. P. Yelisseyev, L. I. Isaenko, U. N. Roy, A. Burger, K. C. Mandal, and K. Nitsch, "Optical properties of $Nd^{3+}$- and $Tb^{3+}$-doped $KPb_2Br_5$ and $RbPb_2Br_5$ with low nonradiative decay," J. Opt. Soc. Am. B **21**, 2117–2129 (2004).
20. H. Sakr, D. Furniss, Z. Tang, L. Sojka, N. A. Moneim, E. Barney, S. Sujecki, T. M. Benson, and A. B. Seddon, "Superior photoluminescence (PL) of $Pr^{3+}$-In, compared to $Pr^{3+}$-Ga, selenide-chalcogenide bulk glasses and PL of optically-clad fiber," Opt. Express **22**, 21236–21252 (2014).
21. M. Pollnau and S. Jackson, "Advances in mid-infrared fiber lasers," in *Mid-Infrared Coherent Sources and Applications*, M. Ebrahim-Zadeh and I. Sorokina, eds. (Springer, 2008), pp. 315–346.
22. B. J. Eggleton, B. Luther-Davies, and K. Richardson, "Chalcogenide photonics," Nat. Photonics **5**, 141–148 (2011).
23. M. Bernier, V. Fortin, N. Caron, M. El-Amraoui, Y. Messaddeq, and R. Vallée, "Mid-infrared chalcogenide glass Raman fiber laser," Opt. Lett. **38**, 127–129 (2013).
24. J. Hu, C. R. Menyuk, C. Wei, L. B. Shaw, J. S. Sanghera, and I. D. Aggarwal, "Highly efficient cascaded amplification using $Pr^{3+}$-doped mid-infrared chalcogenide fiber amplifiers," Opt. Lett. **40**, 3687–3690 (2015).
25. S. D. Jackson, "Towards high-power mid-infrared emission from a fibre laser," Nat. Photonics **6**, 423–431 (2012).
26. Z. Tang, V. S. Shiryaev, D. Furniss, L. Sojka, S. Sujecki, T. M. Benson, A. B. Seddon, and M. F. Churbanov, "Low loss Ge–As–Se chalcogenide glass fiber, fabricated using extruded preform, for mid-infrared photonics," Opt. Mater. Express **5**, 1722–1737 (2015).

126.243.2.47 {ts '2019-03-25 07:20:22'}